Collisions of dark solitons in optical fibers

R. N. Thurston and Andrew M. Weiner

Bellcore, Red Bank, New Jersey 07701-7040

Received September 5, 1990; accepted September 27, 1990

We report numerical simulations that lay the groundwork for possible experiments aimed at the observation of dark soliton collisions. Such experiments would confirm that one can synthesize the appropriate phase functions to launch gray solitons and would test whether an actual collision is adequately described by the nonlinear Schrödinger equation. Our simulations include the effects of a finite-width background pulse and of the Raman contribution to the nonlinear index. We conclude that the observation of dark soliton collisions in optical fibers should be possible, and we indicate suitable experimental parameters.

1. INTRODUCTION

This paper reports numerical simulations that lay the groundwork for possible experiments aimed at the observation of dark soliton collisions. Such experiments would confirm that one can synthesize the appropriate phase functions to launch gray solitons and would test whether an actual collision is adequately described by the nonlinear Schrödinger equation (NLSE).

Hasegawa and Tappert[1] predicted bright and dark solitons in optical fibers in the regimes of anomalous (negative) and normal (positive) group-velocity dispersion (GVD), respectively. Bright solitons in optical fibers were first observed more than ten years ago,[2,3] and their collisions and interactions were studied both theoretically[4,5] and experimentally in the temporal[6] as well as the spatial domains.[7,8] Recently, bright soliton propagation over a 10,000-km distance was achieved by using Er-doped fiber amplifiers to compensate for fiber loss.[9] Dark solitons remained a mathematical curiosity until approximately two years ago, when techniques for controlling both the phase and amplitude of subpicosecond pulses were applied in order to generate odd-symmetry dark pulses that propagated unmistakably as solitons.[10,11] The earlier experiments of Emplit *et al.*[12] recognized the necessary condition of odd symmetry but did not show clearly that the dark pulse propagated as a soliton. Krokel *et al.*[13] showed that an even dark pulse evolved into a pair of low-contrast dark solitons. Dark *spatial* solitons were also recently studied experimentally.[14,15] To date, however, there have been no experiments to our knowledge on the interactions of dark temporal solitons.

In 1985 Blow and Doran[16] published analytical solutions for multiple dark solitons on an infinite background, noting that, in contrast to bright solitons, multiple dark solitons do not form bound states and their interaction is simpler. We choose to study the problem numerically in order to include the effects of perturbations that were observed in single dark soliton propagation experiments. In particular, we assess the effects of a finite-duration background pulse[17] and the Raman contribution to the nonlinear index[18–20] on dark soliton collisions.

Previous numerical[17] and experimental[10] studies showed that dark pulses in finite-width background pulses can still propagate as dark solitons, although the solitons broaden adiabatically as the background diminishes in amplitude. Previous studies also revealed temporal and spectral self-shifts of subpicosecond dark solitons, which occurred owing to the Raman contribution to the nonlinear refractive index[18]; these shifts were analogous to Raman-induced spectral shifts of bright solitons.[21] The influence of these perturbations on dark soliton collisions has not previously been examined, to our knowledge.

2. THEORETICAL AND EXPERIMENTAL BACKGROUND

The numerical simulations are solutions of either the standard or the modified NLSE's of Eq. (11) and expression (12) below. In order to relate our results to experiments with particular fiber and pulse parameters, we sketch the following theoretical results.

Figure 1 shows a single dark soliton solution to the standard NLSE with an infinite background assumed. The normalized effective intensity $I(T)$ has the special shape given by the formula[1,11,16,17]

$$I(T) = A^2(1 - B^2 \operatorname{sech}^2 T)/B^2. \tag{1}$$

T is a dimensionless retarded time, given by

$$T = At/t_0 - A^2(1 - B^2)^{0.5}\pi z/2Bz_0. \tag{2}$$

Here t_0 is a characteristic time, A is an amplitude factor such that A^2 is the intensity depth of the hole, and B^2 is a blackness factor related to the contrast. Dark solitons with $B^2 = 1$ have been called black; other dark solitons are called gray.[17] B can range from -1 to $+1$.

When B is between 0 and 1, the phase increases across the pulse, as shown by the solid curve in Fig. 1; with respect to the background light, the gray soliton moves to later times during its propagation. For B between 0 and -1 the opposite is true: The phase is shown by the dashed curve, and the soliton moves toward earlier times during its propagation. The time shift during propagation indicates a propagation speed that is different from the group velocity at the center wavelength. The velocity difference is described quantitatively by the explicit depen-

0740-3224/91/020471-07$05.00 © 1991 Optical Society of America

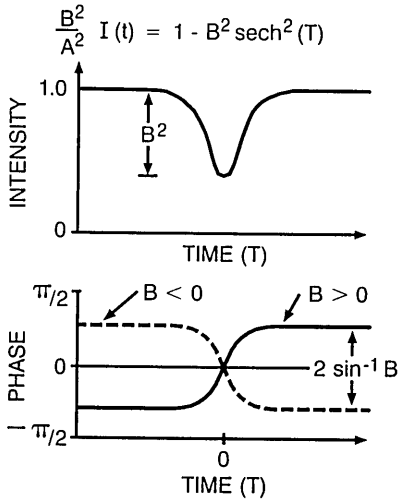

Fig. 1. Gray soliton on an infinite background. (Top) Normalized effective intensity $B^2I(T)/A^2$ versus normalized time T. (Bottom) Phase $\phi(T)$ versus T for $B > 0$ (solid curve) and $B < 0$ (dashed curve).

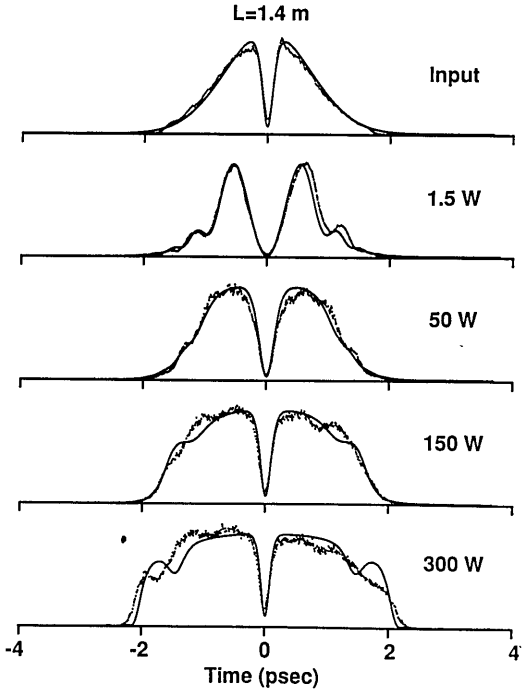

Fig. 2. Propagation of a black ($B^2 = 1$) pulse of initial full width at half-depth (FWHD) 185 fsec on a Gaussian background through 1.4 m of optical fiber at various power levels and superimposed numerical simulations (solid curves), according to the standard NLSE. Data from Ref. 10.

dence of the retarded time T on B in Eq. (2). From Eq. (2)

$$d(t/t_0)/d(z/z_0) = \pi A(1 - B^2)^{1/2}/2B, \tag{3}$$

where T is constant in the differentiation. Since the intensity shape depends only on T, this means that during its propagation the soliton shifts to later times when $B > 0$ and earlier times when $B < 0$.

In Eq. (1)

$$A^2 = P/P_0, \tag{4}$$

where P is the power that corresponds to the soliton depth. P_0 is defined below. The effective intensity $I(T)$ in Eq. (1) is normalized with respect to $I_0 = P_0/A_e$, where A_e is the effective area and P_0 is the power unit that satisfies

$$P_0 z_0 = \pi/2k_2, \tag{5}$$

$$P_0 t_0^2 = |k''|/k_2, \tag{6}$$

$$k_2 = 8\pi^2 n_2 10^7/(\lambda_0 c n_0 A_e), \tag{7}$$

$$k'' = (\partial^2 k/\partial\omega^2)_{\omega_0} = \frac{\lambda_0^3}{2\pi c^2}\left(\frac{d^2 n}{d\lambda^2}\right)_{\lambda_0}. \tag{8}$$

In these definitions n_2 is the coefficient of the refractive-index nonlinearity, $k(\omega, P)$ is the propagation constant in fiber, ω is the radian frequency, λ is the vacuum wavelength, $n(\lambda, P)$ is the refractive index, $n_0 = n(\lambda_0, 0)$, $\lambda_0 = 2\pi c/\omega_0$ is the central wavelength, and c is the speed of light in vacuum in centimeters per second. Additional insight may be gleaned from Refs. 22 and 23. The above normalizations are those used in the classic paper of Tomlinson *et al.*[23] Variations from these normalizations appear in Refs. 16 and 24–26.

The three normalizing units P_0, z_0, and t_0 are connected by only the two independent relations, Eqs. (5) and (6). In solving the standard NLSE, one may arbitrarily choose one of the three units. The other two are then determined by Eqs. (5) and (6). However, when the Raman response function is included, t_0 must be chosen such that the simulated input-pulse envelope has the desired actual time dependence.

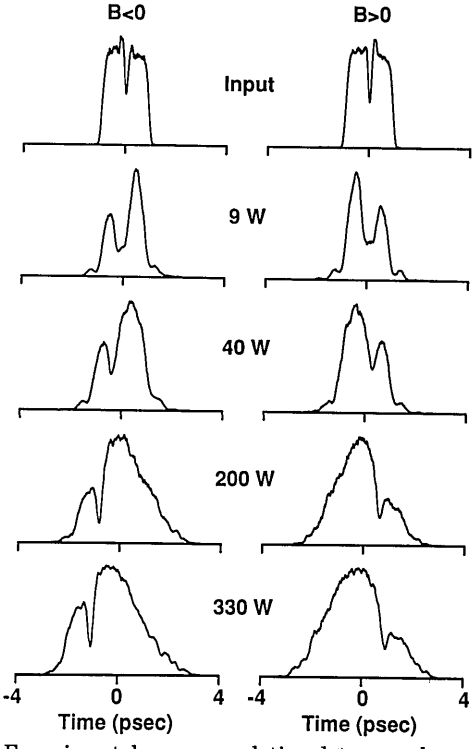

Fig. 3. Experimental cross-correlation data on pulses emerging from a 1.4-m optical fiber with input pulses (top) tailored to propagate as gray solitons with $B < 0$ (left-hand column) and $B > 0$ (right-hand column). $B^2 = 1/2$; initial hole FWHD, 130 fsec. Squarelike background pulse of full width at half-maximum (FWHM) 176 psec. Data from Ref. 11.

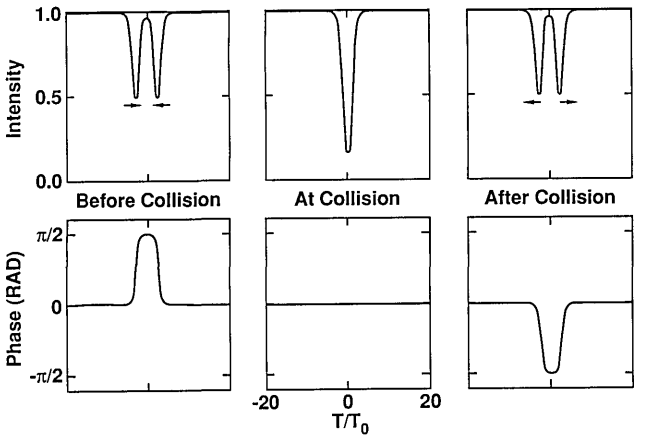

Fig. 4. Normalized intensity (top) and phase (bottom) from numerical simulation of dark-soliton collisions on an infinite background. $B^2 = 1/2$. The slower soliton ($B > 0$) associated with $d\phi/dt > 0$ (higher instantaneous frequency) is launched first (leftmost column). In the middle column, the solitons have merged and their phases cancel each other. In the third column, the solitons have passed through each other, and each of the individual solitons again reveals its associated phase rise or fall.

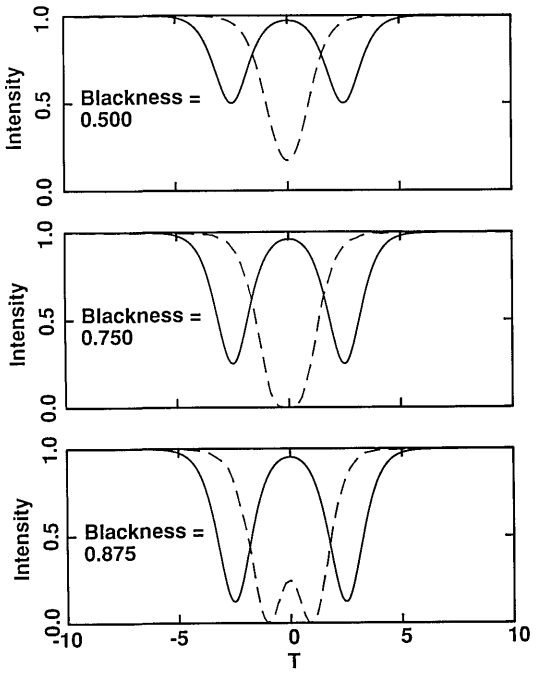

Fig. 5. Normalized intensity versus normalized time from the numerical simulation of dark-soliton collisions on an infinite background with B^2 equal to 1/2 (top), 3/4 (middle), and 7/8 (bottom). The initial intensity profiles (solid curves) have two dips separated by $\delta t = 5t_0$. The dashed profile in each case is at the distance along the fiber where the flat phase (see Fig. 4) indicates coincidence of the two solitons. For $B^2 = 3/4$ or less, the resultant intensity has only a single minimum at the collision distance. For larger B^2 there are two intensity minima at every distance.

The phase $\phi(T)$ is given by

$$\phi(T) = \sin^{-1}\left[\frac{B \tanh(T)}{(1 - B^2 \operatorname{sech}^2 T)^{1/2}}\right]. \tag{9}$$

The complex electric field envelope $E(T, z/z_0)$ enjoys the proportionality[1,11,17]

$$E(T, z/z_0) \propto [I(T)]^{0.5} \exp\left\{i\left[\phi(T) - \frac{\pi A^2 z}{2B^2 z_0}\right]\right\}. \tag{10}$$

The intensity shape as a function of T is independent of z, and, except for the phase lag, which is linear in z, so is the field.

Equations (1) and (9), and expression (10) with the accompanying definitions given above, are solutions of the NLSE, given in the conventional normalized form[23]

$$\frac{\partial a}{\partial(z/z_0)} = i\frac{\pi}{4}\left[\pm\frac{\partial^2 a}{\partial(t/t_0)^2} - 2|a|^2 a\right]. \tag{11}$$

Here $a(t/t_0, z/z_0)$ is a dimensionless complex field amplitude such that the maximum of $|a| = A$ for bright solitons or $A/|B|$ for dark solitons on an infinite background. The $\pm$ sign in Eq. (11) is to be + for positive GVD (dark solitons) and − for negative GVD[27] (bright solitons). We consider only dark solitons below.

One of the assumptions of Eq. (11) is that the nonlinear index changes are simply proportional to the instantaneous intensity. In the formalism of Ref. 20 this is true only for some fraction $(1 - \alpha)$ of the nonlinear index change, while the remaining fraction α follows an impulse response function $f(s)$. To modify the NLSE to incorporate this effect, we replace $|a(z/z_0, t/t_0)|^2$ in Eq. (11) as indicated in expression (12):

$$|a|^2 \to (1 - \alpha)\left|a\left(\frac{z}{z_0}, \frac{t}{t_0}\right)\right|^2 + \alpha\int_{-\infty}^{t}\left|a\left(\frac{z}{z_0}, s\right)\right|^2 f\left(\frac{t}{t_0} - s\right)ds. \tag{12}$$

The Raman impulse response function for vitreous silica

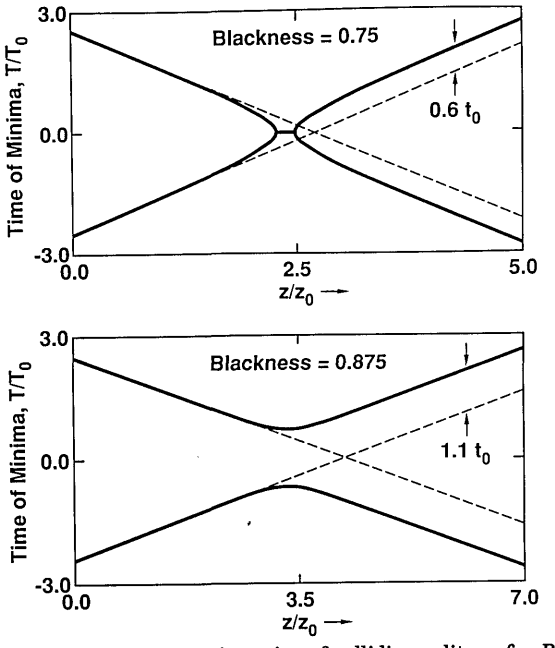

Fig. 6. Distance–time trajectories of colliding solitons for $B^2 = 3/4$ (top) and 7/8 (bottom) on an infinite background. Initial separation $\delta t = 5t_0$. The solid curves show the location of the intensity minima. The dashed lines project where the minima would lie were it not for the other soliton. Far away from the collision site the time difference between the solid line and the associated dashed line is the temporal shift caused by the collision.

Table 1. Graphically Determined Properties of Ideal Dark Soliton Collisions

B^2	Shift during Propagation $d(t/t_0)/d(z/z_0)$		Collision-Induced Shift (units of t_0)	Collision Site (units of z_0)
	Eq. (3)	Graph		
1/4	2.7207	2.717	0.11	0.9
1/2	1.5708	1.605	0.33	1.456
3/4	0.9311	0.904	0.66	2.4
7/8	0.5937	0.594	1.03	3.34
15/16	0.4056	0.407	1.36	4.47

was given by Stolen *et al.*,[20] who also estimated the value $\alpha = 0.18$, the value used in our simulations.

To illustrate the essentials of *single* soliton propagation, we show Figs. 2 and 3. The experiments require control over both the amplitude and the phase of the envelope of the input optical pulse.[10,11,18] Figure 2 illustrates the propagation of a single black pulse on an initially Gaussian background through 1.4 m of optical fiber at various power levels.[10] Both the experimental intensity (points) and numerical simulations are shown. The simulated input intensity actually drops to zero at the center, but all the curves shown have been adjusted to reflect the time resolution present in the experimental measurements, which were obtained by cross-correlation with 75-fsec pulses. The main features seen in Fig. 2 are that at the lowest power the central intensity dip, or hole, broadens because of dispersive linear propagation in the fiber but, as the power increases to the critical power, the width of the hole stabilizes. Thus dark soliton propagation takes place even though the finite-duration background pulse is significantly broadened and diminished in amplitude.

Figure 3 shows experimental cross-correlation data[11] for the pulses exiting a 1.4-m optical fiber; the input pulses were tailored to propagate as gray solitons with $B < 0$ (left-hand column) and $B > 0$ (right-hand column). In this case the input-pulse background was designed to resemble a square pulse. In agreement with the earlier discussion, the hole is shifted to earlier times with $B < 0$ and to later times with $B > 0$. Note, however, that the hole has widened at the lower powers because of GVD. The ability to construct input waveforms that propagate as gray solitons with either positive or negative velocity will be crucial to the experimental observation of gray soliton collisions.

3. IDEAL DARK SOLITON COLLISIONS

A collision can be arranged by launching two dark solitons in succession, the first with positive B and the second with negative B. Then the faster second soliton will overtake the first and merge with it in a collision. The NLSE predicts that after the collision each soliton continues on its way unchanged except for a temporal shift that causes the faster soliton to arrive somewhat earlier (and the slower soliton to arrive somewhat later) than if they passed through each other with no change in velocity during the collision. Our numerical modeling of this situation on an infinite background and without the Raman contribution to the nonlinear index shows that the process goes as just described. From our results we also find the soliton velocity, the distance to the collision (with a specified initial time separation of the solitons), and the temporal shift that is due to the collision. All our simulations used the split-step or beam-propagation method.[28,29]

Before proceeding to the effects of a finite background and the Raman contribution, we examine collisions on an infinite background in Figs. 4–6 and Table 1.

Figure 4 shows both intensity and phase profiles versus normalized time for blackness $B^2 = 1/2$, calculated by the split-step method from the standard NLSE. The initial time separation (left-hand column) is $\delta t = 5t_0$. The collision site can be identified as that distance at which the phase profiles of the two solitons cancel each other to produce a flat resultant phase (middle column), and in the remainder of the paper we use this as a criterion to determine where the collision occurs. Note that at this point the resultant field is a single, even dark pulse. It is instructive to recall that the even pulses of Refs. 13 and 17 split into a pair (or pairs) of gray solitons. The input even pulse itself can be regarded as that same pair (or pairs) in a collision. After the collision (right-hand column) the solitons have separated, and each soliton again carries its own phase rise or fall. It is this phase rise or fall, associated with the instantaneous frequency, that gives the solitons their relative velocity.

Figure 5 shows the resultant intensity profiles before and during collision for three different blacknesses B^2, equal to 1/2, 3/4, and 7/8. The solitons are all launched with an initial time separation $\delta t = 5t_0$. Because the relative velocity depends on B^2, the value of z/z_0 at the collision site $z = z_c$ is different in each case. Note that for $B^2 = 3/4$ the resultant intensity at the collision appears to reach zero at only a single time, but for larger blacknesses there are two times at which the intensity reaches zero at the collision site. Additional calculations show that with values of $B^2 < 3/4$ the resultant depth at the collision site increases with $|B|$; with values of $B^2 > 3/4$ the separation in time of the two minima increases with $|B|$. The resultant intensity $I(T)$ at $z = 2z_c$ is the same as at the input. The combined (resultant) intensity of the two solitons has z as a parameter and can be written as $I(T; z)$. Consider solitons of the same blackness but of opposite B. Then for any z the T dependence is symmetric about $T = 0$, while for any T the z dependence is symmetric about the collision site. In other words, the $I(T; z)$ surface plotted above the (T, z) plane has the intersecting planes of symmetry $T = 0$ and $z = z_c$, where z_c is the coordinate of the collision site.

Figure 6 shows the normalized distance–time paths of the intensity minima of colliding gray solitons for blackness $B^2 = 3/4$ and $B^2 = 7/8$ and initial time separation $5t_0$. The intensity minima follow the solid curves. The dashed lines project the initial paths and hence show where the minima would lie in the absence of the other

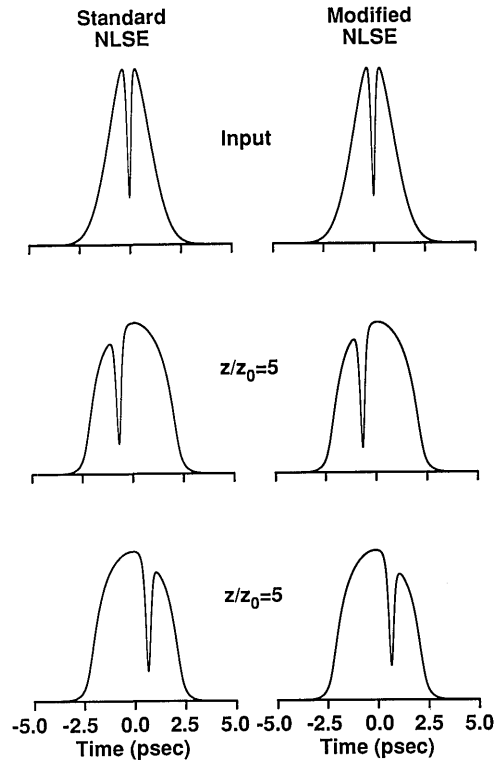

Fig. 7. Intensity versus time for a single gray soliton on an initially Gaussian background. $A = 1$; blackness $B^2 = 3/4$. Numerically modeled intensity input and shapes at $z/z_0 = 5$ for $B < 0$ (middle) and $B > 0$ (bottom). Standard NLSE (left-hand column) and NLSE modified to include the Raman contribution[20] to the nonlinear index (right-hand column).

soliton. The time shift caused by the collision is found from the time difference between the solid curves and dashed lines far from the collision site. The slopes of the dashed lines show the relative velocity of the solitons. Several checks of these slopes were made, and the results agreed in every case with Eq. (3) within the accuracy of the graphical determination (see Table 1). From the observation that the intersection of the dashed lines is somewhat beyond the collision site, one can conclude that the collision occurs at a distance that is less than would be calculated from the initial velocities.

Table 1 lists, for five selected values of B^2, the time shift (rate) during propagation $\mathrm{d}(t/t_0)/\mathrm{d}(z/z_0)$, the time shift due to the collision in units of t_0, and the distance from the input (where the separation is $5t_0$) to the collision site in units of z_0.

From the preceding results one can see that the experimental observation of dark soliton collisions will require a $|B|$ that is neither too large nor too small. Since $\mathrm{d}(t/t_0)/\mathrm{d}(z/z_0)$ decreases with increasing $|B|$, a small $|B|$ is needed to achieve collision in a reasonable fiber length. Since the time shift due to the collision increases with $|B|$, a large $|B|$ is needed to achieve an observable time shift. Thus there will need to be some experimental compromise in the choice of $|B|$. $B^2 = 3/4$ would seem to be a reasonable experimental choice. If we take $t_0 = 127$ fsec and fiber parameters $z_0 = 46.8$ cm, then the entries for $B^2 = 3/4$ in Table 1 show that the collision-induced time shift is 84 fsec and that the collision site is 112 cm from the input.

We digress to note that two colliding particles that repel each other could produce trajectories that are similar to the bottom plot in Fig. 6; but then each particle would follow its own solid curve, indicating a reflection or relative velocity reversal, whereas in the case of colliding dark solitons say that the faster one that enters is the same as the faster one that exits. Is this true: Do they indeed pass through each other, or are they reflected off each other? For solitons of the same $|B|$ this is not a meaningful question. However, for solitons of different $|B|$, we answer the question by numerically colliding two solitons of different blackness. The results support the interpretation that they pass through each other, as is required if the dark pulses are solitons.

4. DARK SOLITON COLLISIONS WITH PERTURBATIONS

The collisions in Figs. 4–6 are all simulated with an infinite cw background. If a dark soliton collision experiment is to be performed by using the experimental approach of Ref. 10, it has to be done with a finite-width background pulse because of the limitations of the femtosecond pulse-shaping technique. Further, if for the chosen parameters the Raman contribution to the nonlinear index is significant, one needs to see how this effect alters the results. To begin to understand these effects, we studied the propagation of a single gray soliton on a finite background both with and without the Raman contribution to the nonlinear index (i.e., with both the standard and the modified NLSE). Figures 7 and 8 illustrate the results.

Figure 7 shows the intensity shapes of a single gray soliton with $B^2 = 3/4$ and a FWHD of 224 fsec in a Gaussian

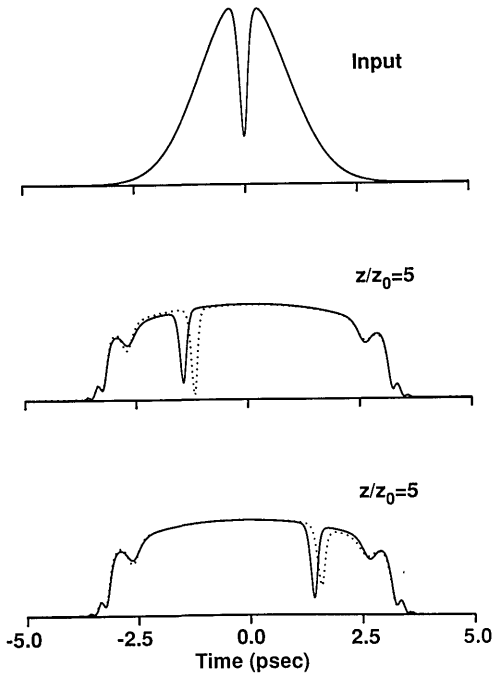

Fig. 8. Single gray soliton on an initially Gaussian background. $A = 2$. Numerically modeled intensity input and shapes at $z/z_0 = 5$ for $B < 0$ (middle) and $B > 0$ (bottom). Superimposed numerical results from the standard (solid curves) and modified[20] NLSE (dotted curves).

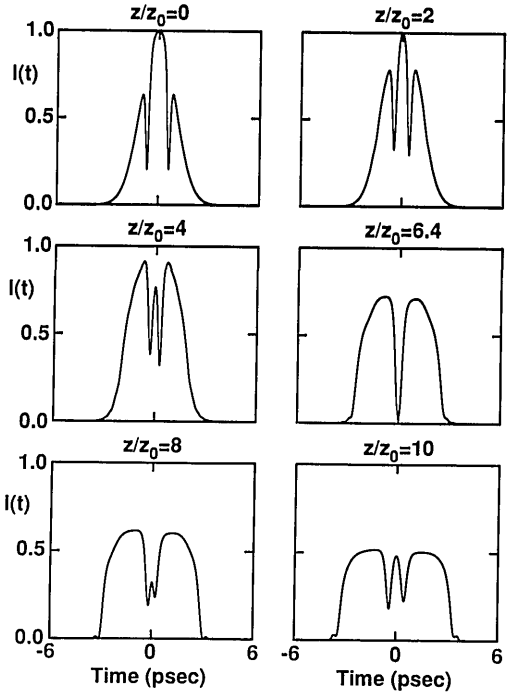

Fig. 9. Collisions of dark solitons on an initially Gaussian background ($B^2 \simeq 3/4$, $A \simeq 1$, but see text). Numerical intensity profiles from the modified NLSE[20] at z/z_0 equal to 0, 2, 4, 6.4, 8, and 10. The collision site is near $z = 6.4z_0$. The initial hole separation is $10t_0$, the initial Gaussian FWHM is $20t_0$, $t_0 = 127$ fsec, the initial hole FWHD is 224 fsec, $z_0 = 0.468$ m, $A_e = 12.56$ μm^2, $\lambda^2 d^2n/d\lambda^2 = 4.9$ at $\lambda_0 = 0.62$ μm. ($k'' = 0.054$ psec^2/m), $n_2 = 1.1 \times 10^{-13}$ cm^2/statvolt^2, $P_0 = 132$ W.

background of initial intensity FWHM of 2.24 psec. (The input field for this calculation is constructed by simply multiplying the field of the idealized soliton on an infinite background by the prescribed Gaussian.) The intensity profiles are shown at the input and after propagating a distance $5z_0$, $z_0 = 0.468$ m. This is approximately twice the distance to the collision site for the idealized case of Table 1. The initially Gaussian background pulse broadens and flattens markedly owing to GVD. The Raman influence is barely discernible, but close inspection of overlays of the plots shows that the soliton that shifts toward earlier times during its propagation becomes slightly deeper and less shifted with the Raman turned on, whereas the soliton with positive B becomes slightly shallower and more shifted. Thus, the Raman contribution causes the $|B|$ to decrease for $B > 0$ and to increase for $B < 0$. When the power is increased by a factor of 4 above the soliton power to $A = 2$, as in Fig. 8, the markedly increased chirping due to self-phase modulation leads to even more broadening of the background pulse. Moreover, the Raman self-frequency shift is greater at higher powers, so that the Raman effects after a propagation distance of $5z_0$ are easily seen.

We note that the effect of the Raman contribution to the nonlinear index on gray soliton propagation was recently described analytically in the perturbation limit by Kivshar.[30] His results are in qualitative agreement with the numerical results reported here and also with the numerical and experimental results of Ref. 18.

Finally, we use the modified[20] NLSE to include the Raman contribution to the nonlinear index in simulating the collision of dark pulses on a finite-width Gaussian bright pulse background. The input field for this calculation is the field of a pair of idealized solitons on an infinite background with $B^2 = 3/4$, $A = 1$, and initial separation $10t_0$ multiplied by a Gaussian pulse of FWHM $20t_0$, $t_0 = 127$ fsec. Since A and B are parameters that are well defined only for the idealized case of a flat background, it is impossible to determine an effective A and B for the input pulse. For this reason, as well as because A and B may change as the background pulse changes, the distance to the collision site cannot be predicted accurately from the data in Table 1 for idealized dark solitons. The intensity shape at the start (where the dark pulses are separated by $10t_0$) and at five distances along the fiber are shown in Fig. 9. The collision site is at $\sim 6.4z_0$. The collision can be tracked even though the background bright pulse is substantially broadened and reduced in intensity during its propagation. Also, the Raman-induced contrast changes appear to occur mainly before the collision without any dramatic change at the collision. (We see also that the solitons do indeed pass through each other rather than reflect, for although the solitons of Fig. 9 have the same $|B|$ at the start, they have become distinguishable before the collision because of the Raman influence.)

CONCLUSION

Since the parameters indicated in the caption of Fig. 9 appear to be experimentally reasonable and since the modified NLSE has in the past proved to be a reliable predictor of experimental dark-pulse behavior,[11,18] we conclude that the experimental observation of dark soliton collisions should be possible.

Taking the parameters of Fig. 9 as an example, we find the initial Gaussian background pulse FWHM to be ~ 2.5 psec, while the holes on an infinite background have a FWHD of 0.224 psec, initially separated by 1.27 psec. The critical power of 132 W corresponds to the depth of the hole, a quantity that is not clearly defined when the background is not flat. On a flat background, with $B^2 = 3/4$ and $A = 1$, the maximum power would be $P_0/B^2 = 176$ W. However, since the intensity height of the Gaussian background field at the hole position in this example is 0.841 times the maximum intensity, one could argue that the peak power of the Gaussian background should be scaled up to approximately 210 W. This is meant only to give a rough indication. The effective parameters will evolve as the background pulse shape and height change. A fiber length of 6 m is approximately twice the anticipated distance to the collision site in the example of Fig. 9. Rather than cleave the fiber to make observations at various distances with an identical input pulse, we may prefer first to see what can be learned with a fixed length of fiber by varying the input pulse parameters. For example, by varying the separation of the input gray solitons we should be able to adjust the collision site in the fiber or even to make the collision distance longer than the physical length of the fiber.

Since the soliton velocity changes as the background intensity changes, the determination of a time shift caused by the collision is not so straightforward as in Fig. 6. Our modeling, using the parameters of Fig. 9, suggests that a collision-induced time shift of ~ 90 fsec is to be expected.

This is less than half of the hole FWHD. It can be increased by increasing the effective $|B|$, but the fiber has to be correspondingly longer (See Table 1).

Finally, we comment on prospects for synthesizing the input waveforms required for observing gray soliton collisions. Inputs that consist of pairs of gray solitons phased to collide within the fiber have a complex-valued frequency spectrum, and this requires gray-level (or continuous) control of the optical phase within the pulse shaping apparatus. Recently a programmable pulse shaping apparatus, based on a multielement liquid-crystal phase modulator, was constructed and used to demonstrate gray level phase control of the optical frequency spectrum.[31] With some further refinement this programmable pulse shaping apparatus should make it possible to synthesize gray soliton waveforms that are suitable for carrying out the collision experiments discussed in this paper.

ACKNOWLEDGMENTS

We thank D. E. Leaird for assistance in preparing the figures and W. J. Tomlinson for valuable comments on the manuscript.

REFERENCES AND NOTES

1. A. Hasegawa and F. Tappert, "Transmission of stationary nonlinear optical pulses in dispersive dielectric fibers. I. Anomalous dispersion," Appl. Phys. Lett. **23,** 142–144 (1973); "Transmission of stationary nonlinear optical pulses in dispersive dielectric fibers. II. Normal dispersion," Appl. Phys. Lett. **23,** 171–172 (1973).
2. L. F. Mollenauer, R. H. Stolen, and J. P. Gordon, "Experimental observation of picosecond pulse narrowing and solitons in optical fibers," Phys. Rev. Lett. **45,** 1095–1098 (1980).
3. L. F. Mollenauer, R. H. Stolen, J. P. Gordon, and W. J. Tomlinson, "Extreme picosecond pulse narrowing by means of soliton effect in single-mode optical fibers," Opt. Lett. **8,** 289–291 (1983).
4. J. P. Gordon, "Interaction forces among solitons in optical fibers," Opt. Lett. **8,** 596–598 (1983).
5. K. J. Blow and N. J. Doran, "Bandwidth limits of nonlinear (soliton) optical communication systems," Electron. Lett. **19,** 429–430 (1983).
6. F. M. Mitschke and L. F. Mollenauer, "Experimental observation of interaction forces between solitons in optical fibers," Opt. Lett. **12,** 355–357 (1987).
7. A. Barthelemy, F. Reynaud, and B. Colombeau, "Single mode soliton beam waveguides," in *Optical Interconnections,* O. D. D. Soares and G. C. Righini, eds., Proc. Soc. Photo-Opt. Instrum. Eng. **862,** 27 (1987); F. Reynaud and A. Barthelemy, "Optically controlled interaction between two fundamental soliton beams," Europhys. Lett. **12,** 401–405 (1990).
8. J. S. Aitchison, A. M. Weiner, Y. Silberberg, M. K. Oliver, J. L. Jackel, D. E. Leaird, E. M. Vogel, and P. W. E. Smith, "Observation of spatial optical solitons in a nonlinear glass waveguide," Opt. Lett. **15,** 471–473 (1990).
9. L. F. Mollenauer, M. J. Newbelt, S. G. Evangelides, J. P. Gordon, J. R. Simpson, and L. G. Cohen, "Experimental study of soliton transmission over more than 10,000 km in dispersion-shifted fiber," Opt. Lett. **15,** 1203–1205 (1990).
10. A. M. Weiner, J. P. Heritage, R. J. Hawkins, R. N. Thurston, E. M. Kirschner, D. E. Leaird, and W. J. Tomlinson, "Experimental observation of the fundamental dark soliton in optical fibers," Phys. Rev. Lett. **61,** 2445 (1988).
11. A. M. Weiner, "Dark optical solitons," in *Optical Solitons: Theory and Experiment,* J. R. Taylor, ed. (Cambridge U. Press, Cambridge, to be published).
12. P. Emplit, J. P. Hamaide, R. Reynaud, C. Froehly, and A. Barthelemy, "Picosecond steps and dark pulses through nonlinear single-mode fibers," Opt. Commun. **62,** 374–379 (1987).
13. D. Krokel, N. F. Halas, G. Giuliani, and D. Grischkowsky, "Dark pulse propagation in optical fibers," Phys. Rev. Lett. **60,** 29–31 (1988).
14. D. R. Andersen, D. E. Hooton, G. A. Swartzlander, Jr., and A. E. Kaplan, "Direct measurement of the transverse velocity of dark spatial solitons," Opt. Lett. **15,** 783–785 (1990).
15. G. R. Allan, S. R. Skinner, D. R. Andersen, and A. L. Smirl, "Observation of fundamental dark spatial solitons in semiconductors using picosecond pulses," Opt. Lett. **16,** 156–158 (1991).
16. K. J. Blow and N. J. Doran, "Multiple dark soliton solutions of the nonlinear Schrodinger equation," Phys. Lett. **107A,** 55–58 (1985).
17. W. J. Tomlinson, Raymond J. Hawkins, A. M. Weiner, J. P. Heritage, and R. N. Thurston, "Dark optical solitons with finite-width background pulses." J. Opt. Soc. Am. B **6,** 329–334 (1989).
18. A. M. Weiner, R. N. Thurston, W. J. Tomlinson, J. P. Heritage, D. E. Leaird, E. M. Kirschner, and R. J. Hawkins, "Temporal and spectral self-shifts of dark optical solitons." Opt. Lett. **14,** 868–870 (1989).
19. R. H. Stolen and E. P. Ippen, "Raman gain in glass optical waveguides," Appl. Phys. Lett. **22,** 276–278 (1973).
20. R. H. Stolen, J. P. Gordon, W. J. Tomlinson, and H. A. Haus, "Raman response function of silica-core fibers," J. Opt. Soc. Am. B **6,** 1159–1166 (1989).
21. F. M. Mitschke and L. F. Mollenauer, "Discovery of the soliton self-frequency shift," Opt. Lett. **11,** 659–661 (1986).
22. R. H. Stolen and Chinlon Lin, "Self-phase-modulation in silica optical fibers," Phys. Rev. A **17,** 1448–1453 (1978).
23. W. J. Tomlinson, R. H. Stolen, and C. V. Shank, "Compression of optical pulses chirped by self-phase modulation in fibers," J. Opt. Soc. Am. B **1,** 139–149 (1984).
24. E. Bourkoff, W. Zhao, R. I. Joseph, and D. N. Christodoulides, "Evolution of femtosecond pulses in single-mode fibers having higher-order nonlinearity and dispersion," Opt. Lett. **12,** 272–274 (1987).
25. W. Zhao and E. Bourkoff, "Propagation properties of dark solitons," Opt. Lett. **14,** 703–705 (1989).
26. L. F. Mollenauer, J. P. Gordon, and M. N. Islam, "Soliton propagation in long fibers with periodically compensated loss," IEEE J. Quantum Electron. **QE-22,** 157–173 (1986).
27. Positive and negative GVD corresponds to the sign of $d^2k/d\omega^2$, where k is the propagation constant and ω the radian frequency. The group velocity $v = d\omega/dk$ decreases as wavelength decreases in the positive regime. Positive dispersion, also called normal dispersion, is observed in vitreous silica in the visible (and in frequency down to the wavelength of zero GVD, $\bar{\lambda}_0$, ~1.3 μm.) In a waveguide, not only the material properties but also geometric factors influence the dispersion. This fact is exploited in order to shift the wavelength of zero GVD, $\bar{\lambda}_0$, in dispersion-shifted fibers. (With normal dispersion a prism bends the violet through a greater angle than the red, as is "normally" observed!) The two kinds of dispersion and their related characteristics are summarized in the following lists: λ is the vacuum wavelength, and the refractive index n is given by $n = ck/\omega$, c being the speed of light in vacuum. For positive (normal) GVD, $d^2k/d\omega^2 > 0$, $dv_g/d\omega < 0$, $dv_g/d\lambda > 0$, $\lambda < \bar{\lambda}_0$, $d^2n/d\lambda^2 > 0$, dark solitons. For the negative (anomalous) GVD, $d^2k/d\omega^2 < 0$, $dv_g/d\omega > 0$, $dv_g/d\lambda < 0$, $d^2n/d\lambda^2 < 0$, $\lambda > \bar{\lambda}_0$, bright solitons.
28. J. A. Fleck, Jr., J. R. Morris, and E. S. Bliss, "Small-scale self-focusing effects in a high power glass laser amplifier," IEEE J. Quantum Electron. **QE-14,** 353–363 (1978).
29. David Yevick and Björn Hermansson, "Soliton analysis with the propagating beam method," Opt. Commun. **47,** 101 (1983).
30. Y. S. Kivshar, "Dark soliton dynamics and shock waves induced by the stimulated Raman effect in optical fibers," Phys. Rev. A **42,** 1757–1761 (1990).
31. A. M. Weiner, D. E. Leaird, J. S. Patel, and J. R. Wullert, "Programmable femtosecond pulse shaping by use of a multielement liquid-crystal phase modulator." Opt. Lett. **15,** 326–328 (1990).